frontiers in
MICROBIOLOGY

ORIGINAL RESEARCH ARTICLE
published: 13 February 2012
doi: 10.3389/fmicb.2012.00041

Characterization of lead–phytochelatin complexes by nano-electrospray ionization mass spectrometry

Christian Scheidegger[1,2], Marc J.-F. Suter[1,2]*, Renata Behra[1] and Laura Sigg[1,2]

[1] Department of Environmental Toxicology, Eawag, Swiss Federal Institute of Aquatic Science and Technology, Dübendorf, Switzerland
[2] Department of Environmental Systems Science, ETH Zürich, Institute of Biogeochemistry and Pollutant Dynamics, Zürich, Switzerland

Edited by:
Martha Gledhill, University of Southampton, UK

Reviewed by:
Jeffrey M. Dick, Curtin University of Technology, Australia
Claude Fortin, Institut National de la Recherche Scientifique, Canada

***Correspondence:**
Marc J.-F. Suter, Department of Environmental Toxicology, Eawag, Swiss Federal Institute of Aquatic Science and Technology, PO Box 611, CH-8600 Dübendorf, Switzerland.
e-mail: marc.suter@eawag.ch

The role of phytochelatins (PC_n, metal-binding oligopeptides with the general structure $(\gamma Glu\text{-}Cys)_n$-Gly ($n = 2$–11) in metal detoxification is assumed to be based on immobilization of metals, which prevents binding of metals to important biomolecules. Although induction of phytochelatin synthesis has often been observed in algae upon exposure to metals, direct evidence for binding of the inducing metal to phytochelatins is scarce. In this study, a nano-electrospray ionization mass spectrometry (nano-ESI-MS) method is developed for identification and characterization of Pb(II)–PC_n and Zn(II)–PC_n complexes. Complexes of Pb(II) with standard PC_n ($n = 2$–4; 0.25 mM Pb(II) and 0.5 mM PC_n) were examined by nano-ESI-MS with respect to their stoichiometry. Pb–PC_n mass spectra indicated the presence of the $[M + H]^+$ peak of PC_n and complexes with various stoichiometries. Analysis of Pb–PC_2 allowed the identification of four different complexes observed at *m/z* 746.10, 952.06, 1285.24, and 1491.20, corresponding to $[Pb\text{–}PC_2]^+$, $[Pb_2\text{–}PC_2]^+$, $[Pb\text{–}(PC_2)_2]^+$, and $[Pb_2\text{–}(PC_2)_2]^+$. Their *m/z* indicated coordination of Pb(II) by PC_2 through the thiol groups of PC cysteine and possibly carboxylic groups. For each of the standard PC_3 and PC_4, two different complexes were observed, corresponding to Pb–PC_3, Pb_2–PC_3, Pb–PC_4, and Pb_2–PC_4. The measured isotopic patterns were for all complexes identical to the theoretical isotopic patterns. Addition of Zn(II) (0.125–5 mM) to previously formed Pb–PC_2 complexes showed the appearance of the $[Zn\text{–}PC_2]^+$ complexes at *m/z* 602.05 and the decrease of the $[Pb\text{–}PC_2]^+$ peak. These findings corroborate the postulated Pb–PC complexes from a previous study using size exclusion chromatography of PC extracted from algae, as well as the concurrent formation of Pb–, Zn–, and Cu–PC complexes in algae.

Keywords: phytochelatin, mass spectrometry, nano-ESI-MS, lead, thiol

INTRODUCTION

Phytochelatins (PCs) are known to be induced in response to exposure to various metals in plants (Rauser, 1995; Zenk, 1996) and algae (Gekeler et al., 1988; Ahner et al., 1995; Le Faucheur et al., 2005; Scheidegger et al., 2011a). These metal-binding oligopeptides with the general structure $(\gamma\text{-Glu-Cys})_n$-Gly ($n = 2$–11) are assumed to bind metals through thiolate coordination and are involved in metal homeostasis and detoxification. The role of PCs in metal detoxification likely results from immobilization of metals, preventing non-specific binding to important biomolecules, followed by the transport of the Me–PC complexes into the vacuole of the algal cell, or its excretion. In our previous studies, induction of phytochelatins by exposure of *Chlamydomonas reinhardtii* to Pb(II) has been observed (Scheidegger et al., 2011a). Binding of Pb(II) to phytochelatins has been postulated based on separation of metal complexes from *C. reinhardtii* by size exclusion chromatography (SEC; Scheidegger et al., 2011b). However, direct evidence for binding of the inducing metal to phytochelatins is scarce. It is therefore of interest to attempt to directly characterize metal–phytochelatin complexes.

Several analytical methods such as chromatographic separation (gel filtration or HPLC) coupled with UV detection, flame atomic absorption spectrometry (AAS), radio-active labeling, differential pulse polarography, and inductively coupled plasma mass spectrometry (ICP-MS) have been used to analyze PC_n and metal–phytochelatin complexes (Me–PC; Grill et al., 1985; Maitani et al., 1996; Leopold and Günther, 1997; Leopold et al., 1999; Vacchina et al., 1999, 2000; Schmoger et al., 2000; Scarano and Morelli, 2002; Cruz et al., 2005; Kobayashi and Yoshimura, 2006). These methods, however, do not provide exact molecular weight, stoichiometry, or composition of Me–PC_n complexes. In most *in vivo* studies focusing on Me–PC complex characterization, Me–PC complexes were isolated by gel filtration and the resulting eluate fractions were further analyzed for PC and metal content. PC detection often involves acidification and derivatization, which lead to dissociation of the Me–PC complexes, followed by HPLC analysis. Based on the detected molecular weight range obtained from gel filtration and the PC oligomers detected by HPLC, assumptions on stoichiometry and composition of the Me–PC complexes can be made; however, unambiguous characterization of Me–PC complexes regarding stoichiometry and composition is not possible with these methods.

A technique to precisely detect and characterize the Me–PC_n complexes is thus required. Several studies reported identification

of Cd–PC, Zn–PC, and As(III)–PC complexes using electrospray ionization mass spectrometry (ESI-MS; Yen et al., 1999; Raab et al., 2005; Navaza et al., 2006; Chekmeneva et al., 2007; Chen et al., 2007; Bluemlein et al., 2008, 2009), but analysis of Me–PC complexes formed with lead has not been reported.

In our previous study, induction of PC_2–PC_4 synthesis by Pb(II) was observed in the green alga *C. reinhardtii* (Scheidegger et al., 2011a). Furthermore, formation of PC_n complexes with Cu, Zn, and Pb, and possible stoichiometric compositions of Pb–PC complexes were postulated based on the molecular weight obtained from SEC (Scheidegger et al., 2011b). Therefore, the aim of the present study is to develop an ESI-MS method to identify and characterize Me–PC_n complexes formed with Pb and to examine the competition with Cu and Zn. Sample composition and ESI-MS conditions to analyze Pb complexes with standard phytochelatins ($n = 2$–4) are optimized. The stoichiometry of the Pb–$PC_{2–4}$ complexes is derived.

MATERIALS AND METHODS

CHEMICALS

$Pb(NO_3)_2$, $CuSO_4$, and $ZnSO_4$ salts, ammonium acetate (NH_4CH_3COO), ammonium carbonate ($(NH_4)_2CO_3$; pH 7), polylysine, and 3-morpholinopropanesulfonic acid (MOPS) used in this study were analytical grade and obtained from Sigma-Aldrich (St. Louis, MO, USA). Phytochelatin standards (PC_2, PC_3, and PC_4) were obtained from Invitrogen (San Diego, CA, USA). Formic acid was a suprapure chemical obtained from Merck (Darmstadt, Germany). Ultrafree-MC centrifugal filters (0.45 µm cut-off) were ordered from Millipore AG (Zug, Switzerland).

SAMPLE PREPARATION

In preliminary experiments the solvent mixture for the analysis of Pb–PC complexes was optimized. The following sample composition resulted in the highest signal intensities in nano-electrospray ionization mass spectrometry (nano-ESI-MS) analysis. The ratio of PC_n to Pb was in the range observed in algal cells (Scheidegger et al., 2011a,b). PC_n and Pb were mixed, resulting in final concentrations of 0.5 mM PC_n and 0.25 mM $Pb(NO_3)_2$ in 100 mM NH_4CH_3COO and 50 mM $(NH_4)_2CO_3$. Complex formation was allowed for 15 min at room temperature. Prior to sample analysis 0.1% formic acid was added (pH 6), followed by sample filtration using an Ultrafree-MC centrifugal filter device with a 0.45-µm cut-off.

For competition experiments between Cu or Zn and Pb, standard Pb–PC_2 complexes were prepared as described and complex formation was allowed, followed by the addition of the Cu or Zn solution. Cu and Zn concentrations added to the Pb–PC_2 complexes were 0.125, 0.25, 0.5, and 5 mM. Acidification was done by addition of 0.1% formic acid. The ratios of Cu and Zn to Pb in the competition experiments were in the range Cu (or Zn): Pb = 0.5–20, and would thus simulate a similar or higher concentration of Cu and Zn than Pb, which may be representative for algal cells.

Mass spectra were acquired and analyzed using the software Xcalibur V2.0.7 (Thermo Fisher Scientific, San Jose, CA, USA). The isotopic distributions for the positively charged molecular ions of Me–PC complexes were generated with the spectrum simulation software integrated in Xcalibur.

NANO-ELECTROSPRAY IONIZATION MASS SPECTROMETRY ANALYSIS OF ME–PC COMPLEXES

Solvent mixture optimization for nano-ESI-MS analysis of Pb–PC_n ($n = 2$–4) were carried out on a API4000 triple quadrupole mass spectrometer (Applied Biosystems, Rotkreuz, Switzerland) with attached nanospray source (Sciex, NanoSpray® III Source, Zug, Switzerland).

Final analysis of Pb–PC_n complexes was carried out on a LTQ Orbitrap XL mass spectrometer (Thermo Fisher Scientific, San Jose, CA, USA). Capillaries for nano-ESI were prepared from coated fused silica tubing (TSP-FS; o.d. 375 µm; i.d. 100 µm; BGB, USA) using a needle puller (Model P-2000, Sutter Instruments Co., Novato, CA, USA). The samples were then analyzed by direct infusion. Between each measurement the syringe was cleaned with MeOH and H_2O.

Prior to analysis of Pb–PC_n complexes, the instrument performance and calibration was checked with polylysine. The flow rate for standard Pb–PC_n complex analysis was 1–3 µL/min. The optimal settings of the mass spectrometer operated in positive electrospray ionization mode were: needle voltage, 1.5 kV; capillary temperature, 200°C; capillary voltage, 11 V; tube lens, 130 V; resolution, 30,000; max. injection time, 100,000 ms; automatic gain control FT, 1×10^6. The spectra were acquired from m/z 300 to 1,600 for Pb–PC_2 and from m/z 300 to 2,000 for Pb–PC_3 and Pb–PC_4. Mass accuracy of the measurement was better than 2 ppm for lower mass ions (<1,000 Da) of signal intensities >10%.

RESULTS

ANALYSIS OF STANDARD Pb–PC_n COMPLEXES

The full-scan mass spectrum of the Pb–PC_2 complexes (**Figure 1**) was dominated by the singly charged $[M + H]^+$ ion of PC_2 at m/z 540.1427, which matches the elemental composition of protonated PC_2 ($C_{18}H_{30}N_5O_{10}S_2$) of 540.1429 with an error <0.2 ppm and shows the expected isotopic distribution with a mass assignment <0.5 ppm for signals higher than 10% relative abundance (data not shown). In addition to the protonated molecular ion peaks at m/z 536.3 and 538.4 were also present (data not shown), probably corresponding to oxidized PC_2. A singly charged PC_2 dimer and its oxidation products could be seen at m/z 1079.2783, 1077.2632, and 1075.2474. The four peaks observed at m/z 746.1034, 952.0641, 1285.2379, and 1491.1964 correspond to the molecular weight of singly charged $[Pb–PC_2]^+$, $[Pb_2–PC_2]^+$, $[Pb–(PC_2)_2]^+$, and $[Pb_2–(PC_2)_2]^+$ complexes (**Figure 1**). Pb–PC_2 and Pb_2–PC_2 were present in sufficient intensity to detect the Pb-specific isotopic pattern of both complexes. The measured isotopic pattern of $[Pb–PC_2]^+$ in the m/z range 740–752 is shown in **Figure 2** (front). The relative intensity of the peaks at m/z 742.11, 744.10, 745.10, and 746.10 was observed in a ratio, which reflects the distribution of Pb isotopes (naturally occurring ratio: ^{204}Pb 1.5; ^{206}Pb 23.6; ^{207}Pb 22.6; ^{208}Pb 52.3%). The measured isotopic pattern matched the theoretical pattern (**Figure 2**, back), with a mass error of 0.7 ppm or better for signals higher than 10%. Similarly, the isotopic pattern observed for $[Pb_2–PC_2]^+$ at m/z 944–958, including the isotopic pattern of two Pb ions, matched the simulated spectra (**Figure 3**), with a mass error of 1.1 ppm or less. The signal intensities of the complexes involving one or two Pb ions and two PC_2 molecules $[Pb_{1–2}–(PC_2)_{2]}$ were too low for isotope pattern detection.

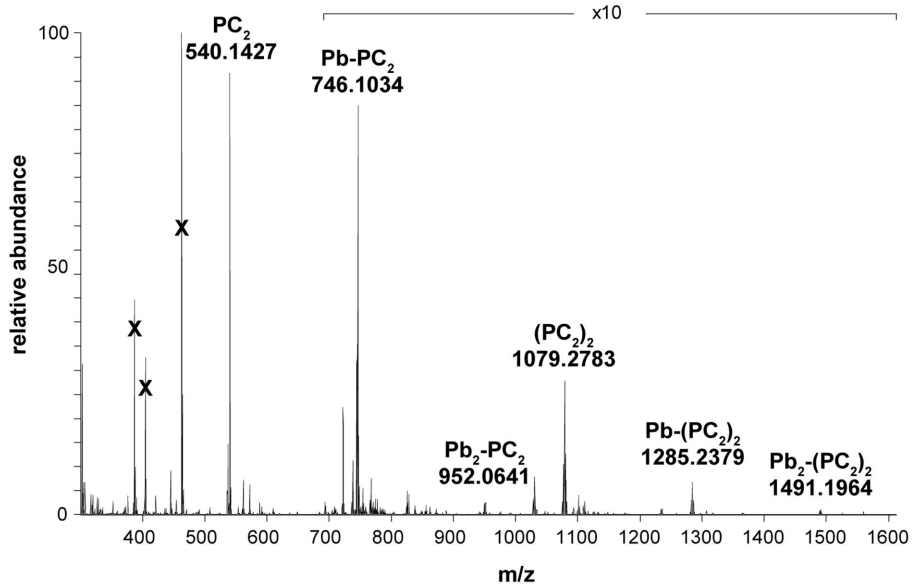

FIGURE 1 | Nano-ESI-MS full-scan spectrum (*m/z* 300–1,600) of 0.5 mM PC_2 ($C_{18}H_{29}N_5O_{10}S_2$) and 0.25 mM $Pb(NO_3)_2$ in 100 mM NH_4CH_3COO, 50 mM $(NH_4)_2CO_3$, and 0.1% HCOOH (pH 6). X = matrix ions.

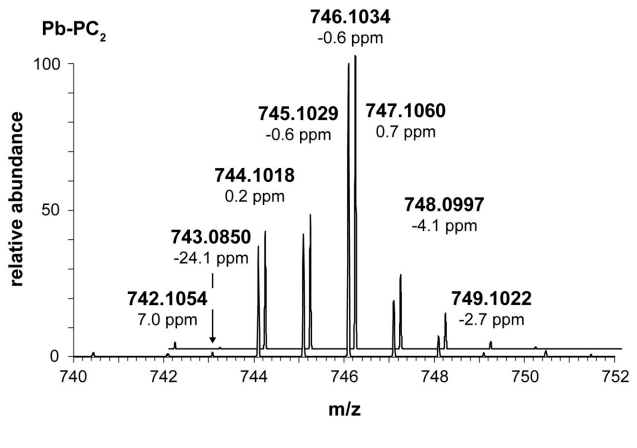

FIGURE 2 | Measured (front) and simulated spectrum (back) of the isotopic pattern of the $[Pb–PC_2]^+$ complex *m/z* 740–752. Isotopic distribution of Pb is identified in the peak distribution at *m/z* 742.11 (^{204}Pb, 1.5%), 744.10 (^{206}Pb, 23.6%), 745.10 (^{207}Pb, 22.6%), and 746.10 (^{208}Pb, 52.3%).

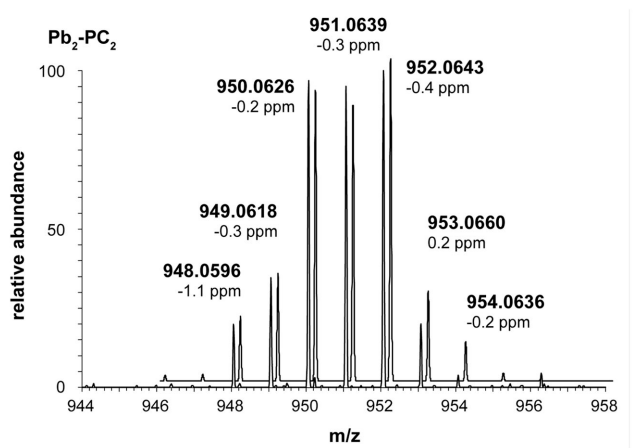

FIGURE 3 | Measured (front) and simulated spectrum (back) of the isotopic pattern of the $[Pb_2–PC_2]^+$ complex *m/z* 944–958. Isotopic distribution of two Pb (^{204}Pb 1.5; ^{206}Pb 23.6; ^{207}Pb 22.6; ^{208}Pb 52.3%) is identified in the peak distribution of the *m/z* 948.06–952.06.

Analysis of $Pb–PC_3$ samples showed the $[M+H]^+$ peak for PC_3 at *m/z* 772.1946 matching the corresponding sum formula ($C_{26}H_{43}N_7O_{14}S_3$; data not shown). Similar to PC_2, a peak at $[M+H\text{-}2]^+$ (*m/z* 770.1790), not present in the theoretical spectra, was present at high signal intensity. Two peaks at *m/z* 978.1559 and 1184.1151 corresponding to the molecular weight of singly charged $[Pb–PC_3]^+$ (mass error 0.3 ppm) and $[Pb_2–PC_3]^+$ (mass error 1.2 ppm) were detected. The measured isotopic pattern and the theoretical spectra were almost identical for both detected complexes (**Figures 4** and **5**).

Analysis of the $Pb–PC_4$ spectra showed the $[M+H]^+$ peak for PC_4 at *m/z* 1004.2406, corresponding to $C_{34}H_{55}N_9O_{18}S_4$. Comparison of the $[M+H]^+$ peak at 1004.2406 for PC_4 to the theoretical spectra shows an excellent match of the isotopic patterns except for the presence of the $[M+H\text{-}2]^+$ peak (*m/z* 1002.2238) as observed for PC_2 and PC_3 and the $[M+H\text{-}4]^+$ peak (*m/z* 1000.2084). Two peaks corresponding to the molecular weight of the PC_4 complexes, $[Pb–PC_4]^+$ and $[Pb_2–PC_4]^+$, were detected at *m/z* 1210.1986 (mass error 7.3 ppm) and 1416.1556 (mass error 8.8 ppm). The measured and theoretical isotopic patterns

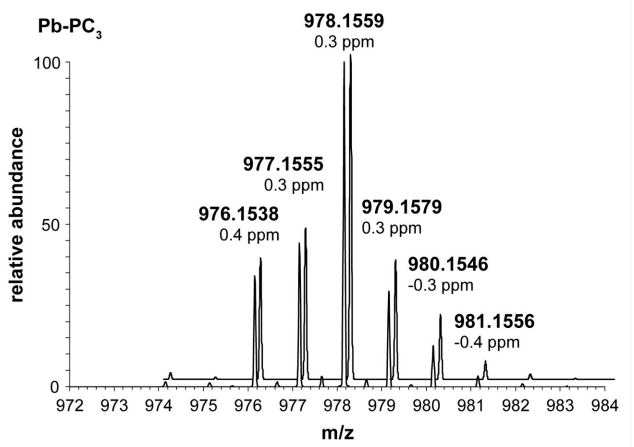

FIGURE 4 | Measured (front) and simulated spectrum (back) of the isotopic pattern of the $[Pb–PC_3]^+$ complex *m/z* 972–984. Isotopic distribution of Pb (^{204}Pb 1.5; ^{206}Pb 23.6; ^{207}Pb 22.6; ^{208}Pb 52.3%) is identified in the peak distribution at *m/z* 974.15, 976.15, 977.15, and 978.16.

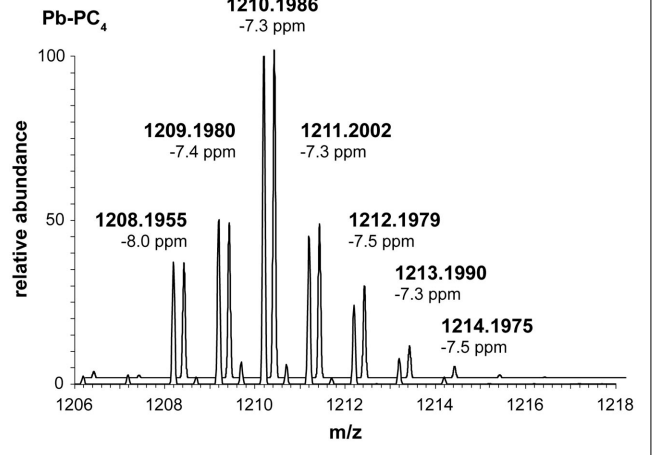

FIGURE 6 | Measured (front) and simulated spectrum (back) of the isotopic pattern of the $[Pb–PC_4]^+$ complex *m/z* 1,206–1,218. Isotopic distribution of Pb (^{204}Pb 1.5; ^{206}Pb 23.6; ^{207}Pb 22.6; ^{208}Pb 52.3%) is identified in the peak distribution at *m/z* 1208.20, 1209.20, and 1210.20.

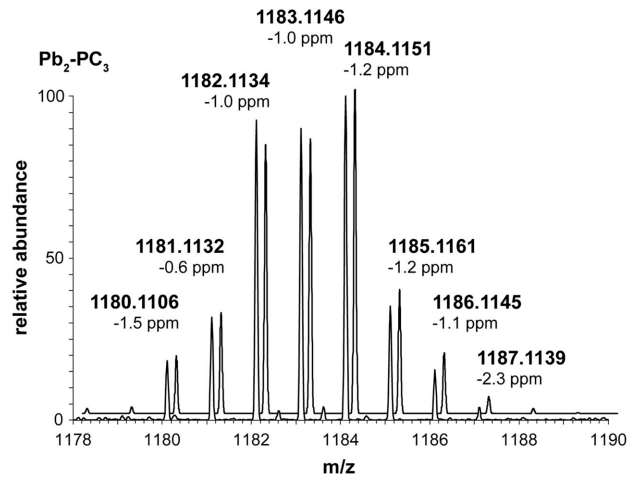

FIGURE 5 | Measured (front) and simulated spectrum (back) of the isotopic pattern of the $[Pb_2–PC_3]^+$ complex *m/z* 1,178–1,190. Isotopic distribution of two Pb (^{204}Pb 1.5; ^{206}Pb 23.6; ^{207}Pb 22.6; ^{208}Pb 52.3%) is identified in the peak distribution of the *m/z* 1180.11–1184.12.

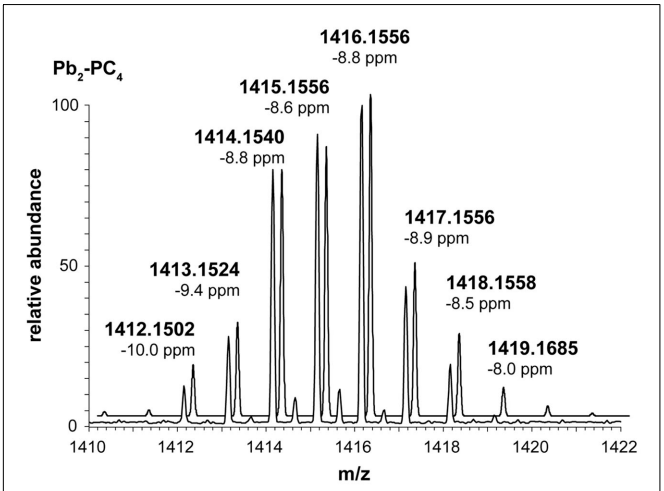

FIGURE 7 | Measured (front) and simulated spectrum (back) of the isotopic pattern of the $[Pb_2–PC_4]^+$ complex *m/z* 1,410–1,422. Isotopic distribution of two Pb (^{204}Pb 1.5; ^{206}Pb 23.6; ^{207}Pb 22.6; ^{208}Pb 52.3%) is identified in the peak distribution of the *m/z* 1412.15–1416.16.

are shown in **Figures 6** and **7**. In addition, a peak at *m/z* 605.6035 was observed, matching the isotopic pattern of $[Pb–PC_4]^{2+}$ (data not shown).

COMPETITION BETWEEN Cu OR Zn AND Pb FOR PC_2 BINDING

Addition of Zn to Pb–PC_2 complexes resulted in the appearance of the $[Zn–PC_2]^+$ peak at *m/z* 602.0544 already at the lowest Zn concentration (**Figure 8A**). In addition, the Pb–PC_2 peak was observed to decrease with increasing Zn concentration (**Figure 8**). Increasing metal concentration leads to a decrease of all PC signals and to an increase of the ratio between the $[M + H]^+$ peak for PC_2 at *m/z* 540.14 and the $[M + H\text{-}2]^+$ peak at *m/z* 538.14. The isotopic pattern of $[Zn–PC_2]^+$ matched with the theoretical distribution of Zn (naturally occurring ratio: ^{64}Zn 48.6; ^{66}Zn 27.9; ^{67}Zn 4.1; ^{68}Zn 18.8; ^{70}Zn 0.6%; **Figure 9**).

At the highest Zn concentration (5 mM) and at all Cu concentrations no Zn–PC or Cu–PC complexes were detected (data not shown).

DISCUSSION

To test the applicability of nano-ESI-MS for the analysis of Me–PC complexes, complexes of Pb with standard PC_n ($n = 2$–4) were analyzed. A method for nano-ESI-MS was developed to characterize *in vitro* formed Me–PC complexes which might also be used for characterization of *in vivo* Me–PC_n complexes.

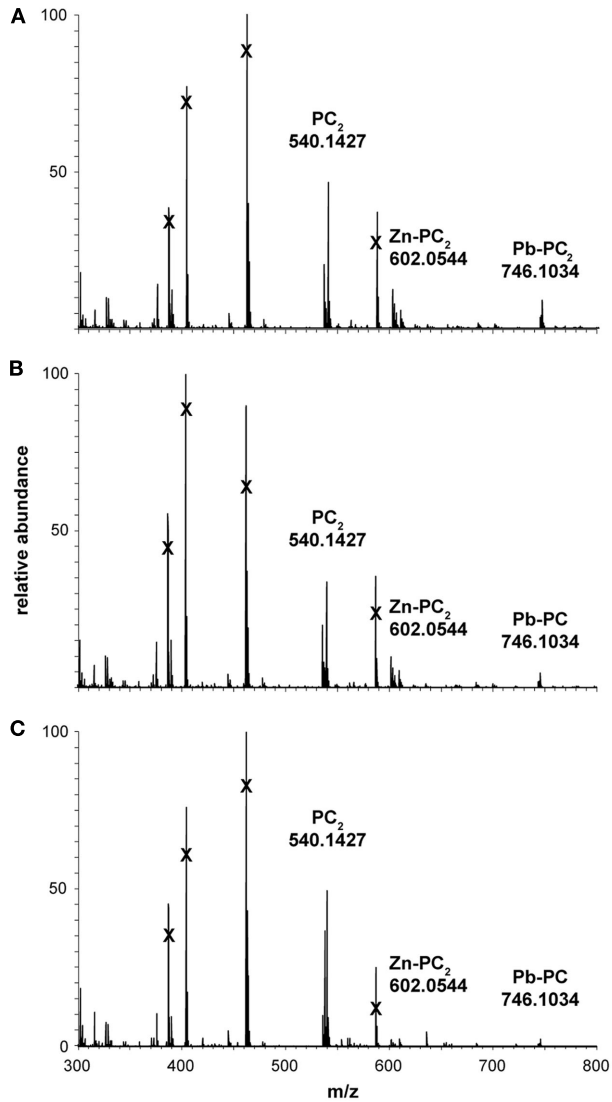

FIGURE 8 | Nano-ESI-MS full-scan spectrum of competition experiments between Pb and Zn with increasing Zn concentrations from (A–C). The concentrations are **(A)** 0.125 mM Zn, **(B)** 0.25 mM Zn, and **(C)** 0.5 mM Zn. X = matrix ions.

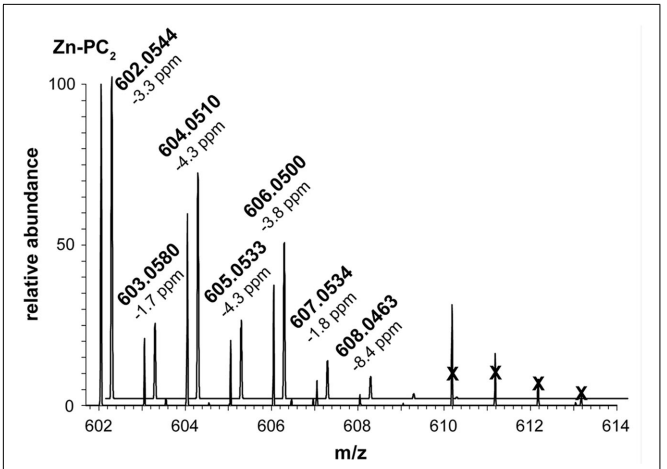

FIGURE 9 | Measured (front) and simulated spectrum (back) isotopic pattern at *m/z* 602–614. Isotopic pattern of Zn (^{64}Zn 48.6; ^{66}Zn 27.9; ^{67}Zn 4.1; ^{68}Zn 18.8; ^{70}Zn 0.6%) and PC_2 is shown at *m/z* 602.05–609.05.

Considering that the mass spectra of the Pb–PC_n complexes were dominated by the $[M + H]^+$ peak of the corresponding PC_n indicates that either not all PC was involved in complex formation, dissociation of Pb–PC complexes occurs during sample analysis, or that the complexes formed were neutral and therefore not visible in the nano-ESI-MS spectra. Furthermore, the relatively low pH 6, needed for optimal ionization, may lead to some complex dissociation.

The PC_n seem to occur mainly in charge state 1+ with the conditions used, as no signal was detected that corresponds to the doubly charged ion. The isotopic pattern of analyzed PC_n was completely resolved. For all PC_n the isotopic distribution matched the theoretical spectra of the corresponding elemental composition and mass accuracy was high (<2 ppm for ions <1,000 Da and with relative intensities higher than 10%). The $[M + H\text{-}2]^+$ peaks observed for PC_2–PC_4 as well as the $[M + H\text{-}4]^+$ peak observed for PC_4, indicate the formation of one or two intramolecular disulfide bonds between cysteine thiol groups within the PC. The formation of a disulfide bond results in a loss of two hydrogens and therefore a shift from $[M + H]^+$ to $[M + H\text{-}2]^+$, which was also observed in other studies (Yen et al., 1999; Navaza et al., 2006).

Analysis of Pb–PC complexes revealed the *in vitro* formation of Pb–PC_n complexes with various stoichiometries and compositions. The *m/z* detected for the $[Pb\text{–}PC_2]^+$ complex allows two different covalent complexes, assuming Pb coordination through thiol groups of PC cysteine. Either Pb is coordinated by one thiol group whereas the other is present as reduced thiol group, or the Pb ion is coordinated by both thiol groups present in PC_2. In the second case, additional protonation of the complex must occur to result in a singly charged complex detectable by nano-ESI-MS. For the $[Pb_2\text{–}PC_2]^+$ complex the detected *m/z* corresponds to $[PC_2 + 2Pb\text{-}3]^+$, indicating a loss of three H^+. This observation suggests that in addition to the two protons from the SH-groups, one proton is lost from a carboxylic group. Further studies would be required to examine whether the complex formation between one Pb and PC_2 involves only thiol groups or Pb is coordinated by one thiol and one carboxylic group. Similarly, another study observed the loss of $2H^+$ and $4H^+$ for the binding of two Cd ions to standard PC_5. Binding of a third Cd ion to PC_5 was not accompanied by the loss of H^+. The authors suggested the formation of complexes that involve two thiol coordinated cadmium ions and a Cd ion which is bound electrostatically to the Cd_2–PC_5 complex (Yen et al., 1999). To investigate whether the coordination of metals by PC is dependent on the metal and/or the chain length of PC needs to be further investigated.

From mass considerations four Pb–PC_2, two Pb–PC_3, and two Pb–PC_4 complexes were identified. To prove that both Pb and PC_n are contributing to the detected signals, the measured isotopic pattern was compared to the theoretical isotopic pattern.

The isotopic patterns of the Pb–PC complexes are complex owing to the isotopic pattern of one or more Pb ions coupled to the PCs (naturally occurring ratio: ^{204}Pb 1.5; ^{206}Pb 23.6; ^{207}Pb 22.6; ^{208}Pb 52.3%). This very pronounced lead signature is indicative for the presence of Pb in the $[Pb–PC_2]^+$ complex at *m*/*z* 740–752. The isotopic pattern of $[Pb_2–PC_2]^+$ is even more complex, since two Pb ions are present in the complex, but comparison of measured and theoretical isotopic pattern proves the presence of the two Pb ions (**Figure 3**). Formation of $[Pb–PC_2]$ and $[Pb_2–PC_2]$ complexes was also observed using differential pulse polarography (Alberich et al., 2007). Similar observations were made for Pb–PC_3 and Pb–PC_4 complexes, showing a good match between measured and theoretical patterns and a loss of $2H^+$ for each additionally bound Pb ion. Surprisingly no complexes including three and four Pb ions were observed for PC_3 and PC_4. These results are also in agreement with the complexes observed using voltammetric methods (Alberich et al., 2008). In addition, accurate mass measurements confirmed the proposed elemental compositions.

The appearance of the $[Zn–PC_2]^+$ peak in the presence of Zn is indicative of complex formation between PC and Zn, which was confirmed by the isotopic pattern for Zn clearly visible in the zoom spectrum (**Figure 9**). This competition between Pb and Zn may be expected if their complex stability with PC_2 is similar to the stability of their complexes with glutathione, for which somewhat higher stability constants for Pb than for Zn are reported (Martell and Smith, 1989). Binding of Zn by PC_3 has been shown in a voltammetric study with multivariate curve resolution, and by PC_4 using voltammetry and ESI-MS (Cruz et al., 2005; Chekmeneva et al., 2007). The expected increase of the $[Zn–PC_2]^+$ peak with increasing Zn concentration was not observed, maybe due to an increase of oxidized PC_2, indicated by the increase of the ratio between *m*/*z* 538.14 and 540.14, leading to a loss of potential metal-binding sites. This could also explain the signal loss observed with increasing Zn concentration. In presence of Cu(II), phytochelatin oxidation may also explain why no Cu–PC complexes were detected. Similar observations were done in a study with Cd where a signal loss was observed at concentrations higher than 0.3 mM Cd (Yen et al., 1999).

In a previous study using SEC, the presence of PC complexes with Cu, Zn, and Pb was postulated upon analysis of PC from *C. reinhardtii* exposed to Pb (Scheidegger et al., 2011b). After extraction of the algal cells under native conditions to preserve the metal complexes, PC_2 and PC_3 complexes were detected in a molecular weight range between 700 and 5,300 Da. PC_2 was mainly observed between 1,000 and 1,600 Da and complexes with $Me_{1–2}–(PC_2)_2$ were suggested, with $[Pb–(PC_2)_2]^+$ and $[Pb_2–(PC_2)_2]^+$ as the probable most abundant Pb species. The results obtained here are in qualitative agreement with this study, as the formation of $[Pb–PC_2]^+$, $[Pb_2–PC_2]^+$, $[Pb–(PC_2)_2]^+$, and $[Pb_2–(PC_2)_2]^+$ is shown. $[Pb–PC_2]^+$ and $[Pb_2–PC_2]^+$ would appear in the SEC fraction 700–1,050 Da, where PC_2 and Pb were also detected. The abundance distribution of these complexes obtained by ESI-MS appears to differ somewhat from the SEC results, but it must be taken into account that the ratio of PC-SH to Pb, as well as the pH were different in these two studies. Furthermore, it must be considered that nano-ESI-MS, albeit a soft ionization technique, may result in dissociation of complexes. The formation of the $[Zn–PC_2]^+$ complex after Zn addition also corroborates the results from SEC, which showed the presence of Zn and Cu, as well as Pb, in the PC containing fractions. These results also clearly indicate a possible competition of Zn and Pb for binding to phytochelatins. These findings support the hypothesis that upon induction of PC_n by Pb in algae, the PC_n may also be bound to other metals.

The application of nano-ESI-MS to examine Me–PC complexes in algae is challenged by practical issues related to the low intracellular concentration of the Me–PC complexes. Therefore, further research is needed to improve the sensitivity for Me–PC complexes by nano-ESI-MS, or respectively to improve sample preparation to obtain a sufficient amount of PC_n from the algae. For example, considering the measured concentration of 30 attomol/cell PC_2 in *C. reinhardtii* cells (Scheidegger et al., 2011a), about 1 L of algal suspension (with a cell density of 8.4×10^5 cell/mL) should be preconcentrated into a small volume (<1 mL) to obtain a sufficiently high PC_2 concentration for ESI-MS measurements. In addition, differences between *in vivo* and *in vitro* formed Me–PC complexes should be further examined to investigate which factors are determining the distribution among the various complexes.

ACKNOWLEDGMENTS

We thank René Schönenberger for help in the laboratory work and the Swiss National Science Foundation for funding this project.

REFERENCES

Ahner, B. A., Kong, S., and Morel, F. M. M. (1995). Phytochelatin production in marine algae. 1. An interspecies comparison. *Limnol. Oceanogr.* 40, 649–657.

Alberich, A., Arino, C., Diaz-Cruz, J. M., and Esteban, M. (2007). Soft modelling for the resolution of highly overlapped voltammetric peaks: application to some Pb-phytochelatin systems. *Talanta* 71, 344–352.

Alberich, A., Diaz-Cruz, J. M., Arino, C., and Esteban, M. (2008). Combined use of the potential shift correction and the simultaneous treatment of spectroscopic and electrochemical data by multivariate curve resolution: analysis of a Pb(II)-phytochelatin system. *Analyst* 133, 470–477.

Bluemlein, K., Raab, A., and Feldmann, J. (2009). Stability of arsenic peptides in plant extracts: off-line versus on-line parallel elemental and molecular mass spectrometric detection for liquid chromatographic separation. *Anal. Bioanal. Chem.* 393, 357–366.

Bluemlein, K., Raab, A., Meharg, A., Charnock, J., and Feldmann, J. (2008). Can we trust mass spectrometry for determination of arsenic peptides in plants: comparison of LC–ICP–MS and LC–ES-MS/ICP–MS with XANES/EXAFS in analysis of *Thunbergia alata*. *Anal. Bioanal. Chem.* 390, 1739–1751.

Chekmeneva, E., Diaz-Cruz, J. M., Arino, C., and Esteban, M. (2007). Binding of $Cd2^+$ and $Zn2^+$ with the phytochelatin (γ-Glu-Cys)(4)-Gly: a voltammetric study assisted by multivariate curve resolution and electrospray ionization mass spectrometry. *Electroanalysis* 19, 310–317.

Chen, L., Guo, Y., Yang, L., and Wang, Q. (2007). SEC-ICP-MS and ESI-MS/MS for analyzing in vitro and in vivo Cd-phytochelatin complexes in a Cd-hyperaccumulator *Brassica chinensis*. *J. Anal. At. Spectrom.* 22, 1403–1408.

Cruz, B. H., Diaz-Cruz, J. M., Arino, C., and Esteban, M. (2005). Complexation of heavy metals by phytochelatins: voltammetric study of the binding of $Cd2^+$ and $Zn2^+$ ions by the phytochelatin (γ-Glu-Cys)3Gly assisted by multivariate curve resolution. *Environ. Sci. Technol.* 39, 778–786.

Gekeler, W., Grill, E., Winnacker, E.-L., and Zenk, M. H. (1988). Algae sequester heavy metals via synthesis of phytochelatin complexes. *Arch. Microbiol.* 150, 197–202.

Grill, E., Winnacker, E. L., and Zenk, M. H. (1985). Phytochelatins: the principal heavy-metal complexing peptides of higher plants. *Science* 230, 674–676.

Kobayashi, R., and Yoshimura, E. (2006). Differences in the binding modes of phytochelatin to Cadmium(II) and Zinc(II) ions. *Biol. Trace Elem. Res.* 114, 313–318.

Le Faucheur, S., Behra, R., and Sigg, L. (2005). Phytochelatin induction, cadmium accumulation and algal sensitivity to free cadmium ions in *Scenedesmus vacuolatus*. *Environ. Toxicol. Chem.* 24, 1731–1737.

Leopold, I., and Günther, D. (1997). Investigation of the binding properties of heavy-metal-peptide complexes in plant cell cultures using HPLC-ICP-MS. *Fresenius J. Anal. Chem.* 359, 364–370.

Leopold, I., Günther, D., Schmidt, J., and Neumann, D. (1999). Phytochelatins and heavy metal tolerance. *Phytochemistry* 50, 1323–1328.

Maitani, T., Kubota, H., Sato, K., and Yamada, T. (1996). The composition of metals bound to class III metallothionein (phytochelatin and its desglycyl peptide) induced by various metals in root cultures of *Rubia tinctorum*. *Plant Physiol.* 110, 1145–1150.

Martell, A. E., and Smith, R. M. (1989). *Critical Stability Constants*. New York: Plenum Press.

Navaza, A., Montes-Bayón, M., Leduc, D. L., Terry, N., and Sanz-Medel, A. (2006). Study of phytochelatins and other related thiols as complexing biomolecules of As and Cd in wild type and genetically modified *Brassica juncea* plants. *J. Mass Spectrom.* 41, 323–331.

Raab, A., Schat, H., Meharg, A. A., and Feldmann, J. (2005). Uptake, translocation and transformation of arsenate and arsenite in sunflower *Helianthus annuus*: formation of arsenic-phytochelatin complexes during exposure to high arsenic concentrations. *New Phytol.* 168, 551–558.

Rauser, W. E. (1995). Phytochelatins and related peptides – structure, biosynthesis, and function. *Plant Physiol.* 109, 1141–1149.

Scarano, G., and Morelli, E. (2002). Characterization of cadmium- and lead-phytochelatin complexes formed in a marine microalga in response to metal exposure. *Biometals* 15, 145–151.

Scheidegger, C., Behra, R., and Sigg, L. (2011a). Phytochelatin formation kinetics and toxic effects in the freshwater alga *C. reinhardtii* upon short- and long-term exposure to lead (II). *Aquat. Toxicol.* 101, 423–429.

Scheidegger, C., Sigg, L., and Behra, R. (2011b). Characterization of lead induced metal-phytochelatin complexes in *Chlamydomonas reinhardtii*. *Environ. Toxicol. Chem.* 30, 2546–2552.

Schmoger, M. E. V., Oven, M., and Grill, E. (2000). Detoxification of arsenic by phytochelatins in plants. *Plant Physiol.* 122, 793–802.

Vacchina, V., Chassaigne, H., Oven, M., Zenk, M. H., and Lobinski, R. (1999). Characterisation and determination of phytochelatins in plant extracts by electrospray tandem mass spectrometry. *Analyst* 124, 1425–1430.

Vacchina, V., Lobinski, R., Oven, M., and Zenk, M. H. (2000). Signal identification in size-exclusion HPLC-ICP-MS chromatograms of plant extracts by electrospray tandem mass spectrometry (ES MS/MS). *J. Anal. At. Spectrom.* 15, 529–534.

Yen, T.-Y., Villa, J. A., and Dewitt, J. G. (1999). Analysis of phytochelatin-cadmium complexes from plant tissue culture using nano-electrospray ionization tandem mass spectrometry and capillary liquid chromatography/electrospray ionization tandem mass spectrometry. *J. Mass Spectrom.* 34, 930–941.

Zenk, M. H. (1996). Heavy metal detoxification in higher plants – a review. *Gene* 179, 21–30.

Conflict of Interest Statement: The authors declare that the research was conducted in the absence of any commercial or financial relationships that could be construed as a potential conflict of interest.

Received: 05 December 2011; accepted: 26 January 2012; published online: 13 February 2012.

Citation: Scheidegger C, Suter MJ-F, Behra R and Sigg L (2012) Characterization of lead–phytochelatin complexes by nano-electrospray ionization mass spectrometry. Front. Microbio. ***3****:41. doi: 10.3389/fmicb.2012.00041*

This article was submitted to Frontiers in Microbiological Chemistry, a specialty of Frontiers in Microbiology.